

UCSF

UC San Francisco Previously Published Works

Title

Polyunsaturated fatty acid-bound alpha-fetoprotein promotes immune suppression by altering human dendritic cell metabolism

Permalink

<https://escholarship.org/uc/item/1c49n38t>

Journal

Cancer Research, 83(9)

ISSN

0008-5472

Authors

Munson, Paul V
Adamik, Juraj
Hartmann, Felix J
[et al.](#)

Publication Date

2023-05-02

DOI

10.1158/0008-5472.can-22-3551

Peer reviewed

Polyunsaturated Fatty Acid-Bound Alpha-Fetoprotein Promotes Immune Suppression by Altering Human Dendritic Cell Metabolism



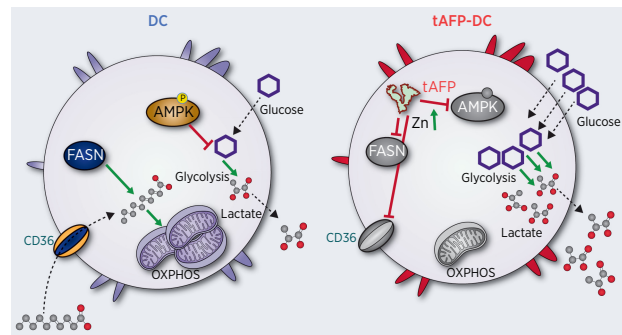
Paul V. Munson^{1,2}, Juraj Adamik^{1,2}, Felix J. Hartmann^{3,4,5}, Patricia M.B. Favaro³, Daniel Ho³, Sean C. Bendall³, Alexis J. Combes^{6,7}, Matthew F. Krummel⁶, Karen Zhang⁷, Robin K. Kelley^{7,8,9}, and Lisa H. Butterfield^{1,2}

ABSTRACT

Alpha-fetoprotein (AFP) is expressed by stem-like and poor outcome hepatocellular cancer tumors and is a clinical tumor biomarker. AFP has been demonstrated to inhibit dendritic cell (DC) differentiation and maturation and to block oxidative phosphorylation. To identify the critical metabolic pathways leading to human DC functional suppression, here, we used two recently described single-cell profiling methods, scMEP (single-cell metabolic profiling) and SCENITH (single-cell energetic metabolism by profiling translation inhibition). Glycolytic capacity and glucose dependence of DCs were significantly increased by tumor-derived, but not normal cord blood-derived, AFP, leading to increased glucose uptake and lactate secretion. Key molecules in the electron transport chain in particular were regulated by tumor-derived AFP. These metabolic changes occurred at mRNA and protein levels, with negative impact on DC stimulatory capacity. Tumor-derived AFP bound significantly more polyunsaturated fatty acids (PUFA) than cord blood-derived AFP. PUFAs bound to AFP increased metabolic skewing and promoted DC functional suppression. PUFAs inhibited DC differentiation in vitro, and ω -6 PUFAs conferred potent immunoregulation when bound to tumor-derived AFP. Together,

these findings provide mechanistic insights into how AFP antagonizes the innate immune response to limit antitumor immunity.

Significance: Alpha-fetoprotein (AFP) is a secreted tumor protein and biomarker with impact on immunity. Fatty acid-bound AFP promotes immune suppression by skewing human dendritic cell metabolism toward glycolysis and reduced immune stimulation.



Introduction

Liver cancer accounts for 8.3% of cancer-related deaths worldwide, making it the third leading cause of cancer-related mortality (1). Hepatocellular carcinoma (HCC) represents 70%–85% of primary

liver cancers (2). Important drivers of HCC rates include chronic hepatitis B (HBV) and C (HCV) infections and control of these infections has decreased HCC rates in East Asia and Southern Europe (3). Unfortunately, downward trends in HBV and HCV infections are offset by increases in other HCC-risk factors, including alcohol consumption, smoking, and obesity. Obesity can lead to fatty infiltration into the liver causing non-alcoholic fatty liver disease (NAFLD), leading to non-alcoholic steatohepatitis (NASH; ref. 4). In the United States, more than 1 in 3 people have some form of NAFLD, and 6 million people have NASH (4). Given HCC's lethality, coupled with the concerning rise in HCC risk factors, new therapies are urgently needed.

Treatments for patients with early stages of HCC include surgery, ablative therapies, embolization approaches, or liver transplantation (5) can be effective. For the majority of patients with more advanced stages of disease, systemic therapy options have expanded in recent years to include small-molecule multikinase inhibitors, monoclonal antibodies targeting VEGF or its receptors, and most recently, immune checkpoint inhibition (6–12)

The combination of bevacizumab and atezolizumab, targeting VEGF and PD-L1, respectively, has emerged as a new global standard for first-line therapy based upon substantial improvement in outcomes compared with the multikinase inhibitor, sorafenib, with median overall survival (OS) of 19.2 months for the combination versus 13.4 months for sorafenib (HR, 0.66; $P = 0.0009$; refs. 9, 13) Objective

¹Parker Institute for Cancer Immunotherapy, San Francisco, California. ²Department of Microbiology and Immunology, University of California San Francisco, San Francisco, California. ³Department of Pathology, Stanford University, Stanford, California. ⁴Systems Immunology and Single-Cell Biology, German Cancer Research Center (DKFZ), Heidelberg, Germany. ⁵Department of Pathology, University of California San Francisco, San Francisco, California. ⁶ImmunoProfiler Initiative, University of California San Francisco, San Francisco, California. ⁷Helen Diller Family Comprehensive Cancer Center, University of California San Francisco, San Francisco, California. ⁸Department of Medicine (Hematology/Oncology), University of California, San Francisco, California. ⁹Cancer Immunotherapy Program, University of California San Francisco, San Francisco, California.

Corresponding Author: Lisa H. Butterfield, University of California San Francisco Medical Center, 1855 Serrano Avenue Street, San Francisco, CA 94109. E-mail: lisa.butterfield@ucsf.edu

Cancer Res 2023;XX:XX–XX

doi: 10.1158/0008-5472.CAN-22-3551

This open access article is distributed under the Creative Commons Attribution-NonCommercial-NoDerivatives 4.0 International (CC BY-NC-ND 4.0) license.

©2023 The Authors; Published by the American Association for Cancer Research

75 responses occurred in 30% of patients treated with the combination of nivolumab and ipilimumab, including 8% with complete responses, with median duration of response not reached. Other immunotherapy combinations have also shown striking improvements in rates of objective radiographic response compared with historical controls (10, 14, 15), and the combination of the PD-L1 inhibitor, durvalumab, with the CTLA-4 inhibitor, tremelimumab, improved OS compared with sorafenib in a randomized, phase III trial (8, 16). These studies demonstrate the potential for robust and durable immune responses in a subset of patients with HCC and underscore the urgent necessity to identify and address mechanisms of resistance in the majority of patients who do not achieve prolonged responses. Although immunotherapies blocking exhaustion markers (PD-1, PD-L1, and CTLA-4) and/or VEGF are encouraging, there are additional barriers *in vivo* that limit the potency of antitumor immunity.

90 Alpha-fetoprotein (AFP) is an oncofetal glycoprotein, similar to albumin, which is expressed by the majority of HCC tumors (tAFP) and can be detected in serum as well as the tumor microenvironment. Elevated serum concentration of AFP is associated with poor prognosis across stages of HCC, and tumors with high AFP expression may represent a distinct biologic subtype associated with activation of proliferative pathways and VEGF signaling (17–19). Like albumin, tAFP is a secreted protein that can bind multiple metabolites and enter activated lymphocytes, hepatocytes, natural killer (NK) cells, and monocytes. Because its initial discovery in a patient with HCC in the 1960s (20), interest in tAFP has focused on its prognostic (21) and diagnostic potential in HCC (22), as a cancer vaccine antigen target (23–25), and its immunoregulatory properties on NK cells (26), macrophages (27, 28), monocytes, and dendritic cells (DC; refs. 29, 30). AFP is also being targeted in TCR-engineered adoptive cell transfer studies (31, 32). Our group demonstrated that tAFP has more potent immunoregulatory properties than cord blood-derived “normal” AFP (nAFP; ref. 29). The molecular features of AFP that are immunoregulatory have been attributed to differences in glycosylation patterns (33, 34), isoforms (35, 36) or isoelectric points (37), and the presence of specific ligands (29, 38–40). In addition, our group has determined that tAFP-mediated suppression of DCs’ function depends on a low molecular mass (LMM; ref. 29) molecule that is neither protein nor glycan.

114 Here, using novel single-cell methods and lipid profiling in both *in vitro* models and *in vivo* human HCC patient blood samples, we have determined that tAFP uptake by DC causes reduced fatty acid uptake and metabolism and a switch to glycolysis accompanied by increased glucose uptake and lactate secretion. This metabolic skewing is accompanied by a shift in immune phenotype, with reduced costimulatory molecule expression and increased DC CD14 and PD-L1 expression. For the first time, we identify differences in the ligand composition between nAFP and tAFP and show that these fatty acids are essential for the immunoregulatory features of tAFP. These findings have important implications for understanding how AFP⁺ HCC limits innate immune responses, identifying strategies to improve DC function *in vivo*, and development of more potent DC vaccines.

128 Materials and Methods

129 Patient samples

130 HCC patient blood (with written informed consent; **Table 1**) and healthy donor (HD) blood [purchased (Trima Residuals RE202, Vitalant)] was collected in BD Vacutainer heparin tubes (Cat # 02–689–6), and in some cases, BD Vacutainer serum tubes (Cat #

Table 1. Characteristics of patients with HCC.

Characteristic (N = 8 patients)	Number or median (range)	(%)
Gender (n)		
Male	6	75%
Female	2	25%
Age, y		
Median (range)	72 (61–83)	
Race		
African-American	2	25%
Asian	2	25%
Caucasian	4	50%
Ethnicity		
Non-Hispanic/Latino	8	100%
Hispanic/Latino	0	0%
Liver Disease Etiology		
Hepatitis C (cAb ⁺)	4	50%
Hepatitis B (sAg ⁺)	2	25%
Child Pugh Score at Enrollment		
Child Pugh A	7	87%
Child Pugh B	1	13%
Serum AFP (μg/L)		
Median (range)	229 (<2.0–7287.9)	
Disease stage		
Stage IIIB	1	13%
Stage IVA	3	38%
Stage IVB	4	50%
Histologic grade		
Moderately differentiated	4	50%
Poorly differentiated	2	25%
Unknown	2	25%

135 B-D367820Z) were collected. Heparinized blood was centrifuged to separate the blood and plasma components. Plasma was stored at 136 –80°C. The remaining cellular fraction was overlaid over Ficoll 137 (Cytiva, Cat# 45–001–749) in Leucosep tubes (Greiner, Cat # 07–138 000–983) and centrifuged to isolate peripheral blood mononuclear 139 cells (PBMC). PBMCs were washed with PBS, and viable cells were 140 quantified via trypan blue (Gibco, Cat # 15–250–061) on a Nexcelom 141 Cellometer Spectrum. If cell pellets had substantial red blood cells, they 142 were briefly lysed using ACK lysing buffer (Thermo Fisher Scientific, 143 Cat #A1049201). Cells were resuspended in freezing media (80% 144 CellGenix + 20% DMSO (MP Biomedicals, Cat #ICN19141880), 145 stored at –80°C overnight, and stored in gas-phase LN₂. 146

147 *In vitro* DC differentiation

148 DCs were differentiated *in vitro* similarly as previously described 149 (29). In brief, cryopreserved PBMCs were thawed and CD14⁺ mono- 150 cytes were magnetically labeled using CD14 MicroBeads (Miltenyi, Cat 151 # 130–050–201) and isolated by LS columns (Miltenyi, Cat # 130–042– 152 401) per the manufacturer’s instructions. Viable eluted cells were 153 enumerated using trypan blue on a Nexcelom Cellometer Spectrum. 154 To generate iDCs, monocytes were stimulated for 5 days in the 155 presence of 800 IU/mL of rGM-CSF (Miltenyi, Cat # 130–093–862) 156 and 500 IU/mL of rIL-4 (Miltenyi, Cat # 130–095–373) as well as OVA, 157 nAFP, or tAFP in CellGenix GMP DC media (Cat #20801–0500) 37°C 158 at 5% CO₂. Highly purified grade tAFP was obtained from Bio-Rad, 159 and the AFP-L3 is approximately 70% as compared with 10% in 160 human cord serum, by PAGE analysis. The nAFP was obtained from 161 Cell Sciences (Cat # CSI0379), with a purity of >99% by SDS-PAGE 162 analysis and sterile filtered. The chicken ovalbumin was obtained by

165	Sigma (Cat # A5503-1G) with a purity of >98% by agarose gel	224
166	electrophoresis. All proteins were aliquoted to prevent multiple	225
167	freeze-thaw cycles and stored at -80C. Finally, an additional 24-hour	226
168	stimulation with 1,000 IU/mL of rIFN γ (Peprotech, Cat #300-02) and	227
169	250 ng/mL of LPS (Sigma-Aldrich, Cat# L2630-10MG) to produce	228
170	monocytic DCs (mDC). To harvest cells, DCs were detached using	229
171	TrypLE Select (Gibco, Cat #12563011) for 15 minutes at 37°C and then	230
172	washed several times with cold PBS.	231
173	SCENITH	232
174	SCENITH was performed as described in ref. (41). The SCENITH	233
175	reagents kit (inhibitors, puromycin and antibodies) was obtained from	234
176	www.scenith.com/try-it and used according to the provided protocol	235
177	for <i>in vitro</i> -derived myeloid cells. Briefly, control and tol-moDC	236
178	cultures at desired timepoints, were treated for 18 minutes with	237
179	Control (DMSO), 2-Deoxy-Glucose (2-DG; 100 mmol/L), Oligomycin	238
180	(O; 1 μ mol/L), a combination of 2DG and Oligomycin (DGO) or	239
181	Harringtonine (H; 2 μ g/mL). Following metabolic inhibitors, Puro-	240
182	mycin (final concentration 10 μ g/mL) was added to cultures for 17	241
183	minutes. After puromycin treatment, cells were detached from wells	242
184	using TrypLE Select (Thermo Fisher Scientific, 505914419), washed in	243
185	cold PBS and stained with a combination of Human  Stain FcX	244
186	(BioLegend, 422301) and fluorescent cell viability dye (BioLegend,	245
187	423105) for 10 minutes 4°C in PBS. Following PBS wash step, primary	246
188	antibodies against surface markers were incubated for 25 minutes at	247
189	4°C in Brilliant Stain Buffer (BD Biosciences, 563794). Next, cells	248
190	were fixed and permeabilized using True-Nuclear Transcription	249
191	Factor Buffer Set (BioLegend, 424401) as per the manufacturer's	250
192	instructions. Intracellular staining of puromycin and protein targets	251
193	was performed for 1 hour in diluted (10x) permeabilization buffer at	252
194	4°C. Finally, data acquisition was performed using the Cytek	253
195	Aurora flow cytometer. Primary conjugated antibody information	254
196	used in SCENITH panel is listed in Supplementary Table S1. All	255
197	antibodies were titrated to reduce spillover and increase resolution	256
198	using single-stained moDC (generated as described above) samples.	257
199	Unstained cell controls used for autofluorescence extraction were	258
200	generated for each time point, culture conditions (OVA, nAFP, and	259
201	tAFP) and metabolic inhibitor treatments (C, 2DG, O, DGO).	260
202	Samples were unmixed using reference controls generated in com-	261
203	bination with stained Ultracomp beads (Thermo Fisher Scientific,	262
204	01-2222-41) and stained cells using the SpectroFlo Software	263
205	v2.2.0.1. The unmixed FCS files were used for data processing and	264
206	analysis using FlowJo (BD Biosciences, version 10.7.1). Manually	265
207	gated CD14 ⁺ HLA-DR ⁺ CD86 ⁺ cells were used for downstream	266
208	analysis. gMFI expression values were imported into R environment	267
209	for correlation and heatmap analysis.	268
210	Glucose and lactate measurements	269
211	Glucose and lactate were measured by applying approximately 5 μ L	270
212	of supernatant to Clarity BG1000 Blood Glucose strips (Cat #75840-	271
213	798) and meter (Cat #75840-800) system or the Lactate Plus strips	272
214	(Nova Biomedical, Cat# 40813) and meter version 2 (Nova Biomedical,	273
215	Cat# 62624) system. Each meter was quality checked with control	274
216	glucose and lactate solutions and CellGenix media before each	275
217	experiment.	276
218	CyTOF phenotypic profiling	277
219	scMEP (single-cell metabolic profiling) analysis was performed as	278
220	recently described in ref. (42). In short, antibodies targeting metabolic	279
221	features were conjugated in-house using an optimized conjugation	280
222	protocol (Hartmann and colleagues, ref. 42) and validated on multiple	281
	sample types. Cells were prepared for scMEP analysis by incubation	
	with small molecules to be able to assess biosynthesis rates of DNA,	
	RNA and protein, cisplatin-based live/dead staining, PFA-based cell	
	fixation and cryopreservation (dx.doi.org/10.17504/protocols.io.	
	bkwkkxcw). Next, cells were stained with metabolic antibodies in	
	a procedure that includes surface staining for 30 minutes at room	
	temperature (RT), PFA-fixation for 10 minutes at RT, MeOH-based	
	permeabilization for 10 minutes on ice, intracellular staining for	
	1 hour at RT and DNA intercalation (dx.doi.org/10.17504/protoc-	
	ols.io.bntnmeme). Finally, cells were acquired on a CyTOF2 mass	
	cytometer (Fluidigm). Protein targets and antibody information	
	used in scMEP are listed in Supplementary Table S2. Raw mass	
	spectrometry data were pre-processed, de-barcoded and imported	
	into R environment using the flowCore package (version 2.0.1;	
	ref. 43). Values were arcsinh transformed (cofactor 5) and normal-	
	ized (42) for downstream analyses based on previously reported	
	workflow (44).	
	Microarray and gProfiler	
	OVA, nAFP, and tAFP-treated DC were lysed, and total mRNA	
	was obtained for microarray (Affymetrix HG-U133A). DE genes	
	were uploaded in g:Profiler in R Studio for pathway analysis and	
	visualization (45).	
	Zn measurement	
	Intracellular Zn was quantified by flow cytometry using the Zinc	
	Assay Kit (Cell-based; Abcam, Cat #ab241014). Monocytes were	
	differentiated to iDCs as described above in the presence of OVA,	
	nAFP, tAFP, or ZnSO ₄ . Zn staining was performed per the manu-	
	facturer's suggested protocol with positive (Zn) and negative (Zn +	
	chelator) controls as well as a Zn FMO included in each experiment.	
	Cells were stained with LD Aqua for 10 minutes at RT. Cells were	
	washed in 1X Assay Buffer, then stained in 100 μ L of Assay Buffer + 0.2	
	μ L of Zn Probe for 30 minutes at 37°C. Cells were then washed	
	twice with 1X Assay buffer then stained with HLA-DR-APC-H7 (BD,	
	Clone: GF6-6, Cat #561358, Lot #0023290, 0339025), CD86-BV785	
	(BioLegend, Clone : IT2.2, Cat # 305441, Lot # B277560), CD206 PE-	
	Cy7 (BioLegend, Clone : 15-2, Cat # 321123, Lot #B331254), and	
	CD14-BUV805 (BD Biosciences, Clone : M5E2, Cat # 612903, Lot	
	#0297714), in Brilliant Stain Buffer (BD Horizon, Cat # 566349, Lot #	
	0121427) for 20 minutes at 4°C. Cells were washed twice in FACS	
	Buffer and fixed in 1% paraformaldehyde (Thermo Fisher Scientific,	
	Cat #J19943-K2, Lot # 195273, diluted in PBS) for at least 30 minutes	
	before acquisition on a BD LSRFortessa X-50. As a negative control, we	
	briefly treated cells with Zn but did not stain for Zn as a fluoresce-	
	minus-one (FMO) control (MFI = 421) or stained with a Zn probe as a	
	positive control (MFI = 25,850). Zn-treated cells were treated with a	
	Zn chelator included in the kit before staining, and this resulted in a	
	marked approximately 97% reduction in Zn MFI compared with the	
	positive control.	
	Lipid analysis by mass spectrometry or gas chromatography	
	Commercially available OVA (N = 3; Sigma-Aldrich, Cat # A5503-	
	1G, Lot # SLCB8249), nAFP (N = 3; Cell Sciences, Cat # CSI10379, Lot	
	# 4111714), and tAFP (N = 3; Bio-Rad, Cat #13752600, Lot #	
	64110896) were submitted diluted in PBS (Gibco, Cat #20-012-	
	050) at 1,000 μ g /mL on dry ice. CellGenix GMP DC Medium	
	(N = 1; CellGenix, Cat #20801-0500) media and supernatants of	
	mDCs from an HD (N = 1) differentiated in the presence of 5 μ g per	
	mL of OVA, nAFP, or tAFP were tested. Lipid analysis (Supplementary	
	Table S1) was performed at the UCSD Lipidomics Core (46).	

284 **Fatty acid screen**

285 Fatty acids (Supplementary Table S3) were acquired from Cayman
 286 Chemical, including **16:0** (palmitic acid, Item # 10006627, Batch #
 287 0523612–48), **18:1** (oleic acid, Item #90260, Batch #0540276–62), **20:3**
 288 **N6** (dihomo- γ -linolenic acid, Item #90230, Batch #0532009–37), **20:3**
 289 **N9** (5,8,11-eicosatrienoic acid, Item #90190, Batch #0564724–7), **20:4**
 290 (arachidonic acid, Item #90010, Batch #0570304–50), **22:4** (adrenic
 291 acid, Item #90300, Batch #0537603–20), **20:5** (eicosapentaenoic acid,
 292 Item #26415, Batch #0583627), **22:5 N3** (docosapentaenoic acid, Item
 293 #90165, Batch #0569492–11), **22:5 N6** (docosapentaenoic acid, Item
 294 #10008335, Batch #0462864–36), and **22:6** (docosahexaenoic acid,
 295 Item #90310, Batch #0593448–15).

296 Fatty acids were resuspended in ethanol and stored at -20°C at
 297 100 $\mu\text{mol/L}$. High molar mass (HMM) fractions of OVA, nAFP, and
 298 tAFP were obtained by removing the LMM contents with the
 299 Amicon Ultra – 0.5 mL Centrifugal Filters Ultracel—3K (Millipore,
 300 Cat #UFC500324, Lot #R9HA51100) per the manufacturer's sug-
 301 gested protocol and stored at -80°C . Both the native preparations
 302 and HMM fractions contained similar amounts of protein
 303 (~ 0.5 mg/mL), whereas protein was undetectable (<0 mg/mL) in
 304 the LMM fraction. In addition, we determined the A_{260}/A_{280} ratio as
 305 a measure of purity and found the LMM fraction had an approx-
 306 imately 3-fold increase in the A_{260}/A_{280} ratio indicating a large
 307 proportion of non-protein compounds in the LMM fraction, as
 308 expected. Fats (\pm HMM) were added to pre-warmed media and
 309 incubated for 1 hour, mixing at 37°C before adding to cells (47).
 310 Fats were combined with HMM at a 3:1 molar ratio, as previously
 311 described (47).

312 **Statistical analysis and visualization**

313 Statistical comparisons between groups were performed using
 314 paired-sample *t* tests unless otherwise stated using R (version 4.0.2)
 315 and R Studio (Version 1.3.1093) or Prism (Version 9.0.2). *P* values
 316 are represented as *, $P \leq 0.05$; **, $P \leq 0.01$; ***, $P \leq 0.001$; ****, $P \leq$
 317 0.0001 . *P* values of <0.05 were considered statistically significant.
 318 Numerical labels indicate near significant values). Figure graphs
 319 were generated using the R package ggplot2 (version 3.3.3) or in
 320 Prism.

321 **Study approval**

322 Blood collection from patients with HCC was approved by the
 323 UCSF Hepatobiliary Tissue Bank and Registry Oversight Commit-
 324 tee (CC#124512). The UCSF Cancer Immunotherapeutics Tissue
 325 Use Committee approved samples from HDs at UCSF (CC#16983).

326 **Data availability statement**

327 The data generated in this study as well as data from prior pub-
 328 lications are available upon request from the corresponding author.
 329 The array data discussed in this publication were previously deposited
 330 in NCBI's Gene Expression Omnibus and are accessible through GEO
 331 Series accession number GSE62005 (<http://www.ncbi.nlm.nih.gov/geo/query/acc.cgi?acc=GSE62005>)"

333 **Results**334 **tAFP induces immunometabolic dysregulation of DCs**

335 To determine the mechanism of immune suppression induced by
 336 AFP, we performed immune and metabolic profiling human DC.
 337 Previously, we demonstrated using population-based assays that tAFP
 338 decreases the differentiation mDCs and reduces their T-cell stimula-
 339 tory potential (29). We demonstrated that tAFP limited DC HLA-DR

and CD206 expression with a trend for reduced CD86. Furthermore,
 the Boolean analysis revealed a decreased co-expression of multiple
 activation markers (HLA-DR, CD206, CD86, and ICOSLG/CD275)
 among tAFP-treated DC.

To understand the immuno-metabolic impact of tAFP on DCs at
 the single-cell level, we used the recently described single-cell
 energetic metabolism by profiling translation inhibition (SCE-
 NITH) assay (41). Ovalbumin (OVA, negative control), nAFP, and
 tAFP-treated DCs were generated *in vitro* (Fig. 1A). Viable cells
 (LD^{-}) actively translating RNA into protein (Puro $^{+}$) were analyzed
 (Supplementary Fig. S1) that expressed cell surface molecules
 associated with mDCs (HLA-DR $^{+}$, CD206 $^{+}$, CD86 $^{+}$; previously
 shown to be representative of many common DC phenotypic
 markers; ref. 30). To assess the broad immuno-metabolic state of
 the cells, a tSNE analysis was performed on all parameters that
 indicated tAFP-treated cells tended to cluster separately from nAFP
 or OVA-treated mDCs. The calculated metabolic profiles are shown
 for glucose dependency, mitochondrial dependency, glycolytic
 capacity, and fatty acid and glutaminolysis (FAAO; Fig. 1B). Even
 among mDC with strong expression of activation markers (HLA-
 DR $^{+}$, CD206 $^{+}$, and CD86 $^{+}$), there was a dramatic increase in
 glycolysis and a reduction in mitochondrial dependency and FAAO
 in tAFP-treated DCs. Consistent with a greater reliance on glycol-
 ysis, tAFP-treated cells had significantly less glucose in culture
 supernatants at day 6 (Fig. 1C). OVA and nAFP-treated DCs had
 relatively higher frequencies of pAMPK $^{+}$ DCs, which is consistent
 with their increased mitochondrial dependency and mitochondrial
 mass as opposed to tAFP-treated DCs. This result is consistent
 with our previous study, in which increased pAMPK signaling as
 opposed to mTOR activation upregulated mitochondrial metabo-
 lism and FAAO in DCs (48). In conjunction with a decrease in
 FAAO, a decline in expression of the fatty acid transporter CD36
 was detected (Fig. 1D). Similarly, free fatty acids in the culture
 supernatants at day 6 were inversely correlated ($r = -0.7110$, $P =$
 0.0318) with the expression of CD36. Taken together, these data
 indicate that tAFP-treated DCs rely on glycolysis and have a
 decreased ability to take up and oxidize fatty acids.

In agreement with decreased mitochondrial capacity by SCE-
 NITH (Fig. 1B), we previously confirmed decreased mitochondrial
 mass in tAFP-treated DCs (30). With decreased mitochondrial
 activity and the DC reliance on glycolysis, we investigated the
 potential release of lactate. Given the immunoregulatory functions
 of lactate, we determined whether tAFP could promote lactate
 secretion by DC. Lactate was measured in the media of OVA,
 nAFP, and tAFP-treated DCs (Fig. 1D). In all HDs, tAFP-treated
 DC secreted the most lactate at approximately twice the concen-
 tration of OVA-treated DCs, which may in part explain tAFP-
 treated DCs diminished capacity to stimulate T cells (29). The
 increased concentrations of lactate inversely correlated with glucose
 in the supernatant ($r = -0.9326$, $P = 0.0002$), suggesting this build-
 up of lactate results from increased reliance on glycolysis, as
 opposed to oxidative phosphorylation or FAAO, for the production
 of ATP.

Given that tAFP induced both immune and metabolic changes, we
 examined correlations between costimulatory markers and metabolic
 state. Cells were gated on the basis relative mitochondrial mass (Fig. 2).
 As mitochondrial size decreased, the cells coalesced around a single
 cluster. To determine the impact of altered mitochondrial load on
 the expression of key costimulatory molecules, we determined the
 relative expression of activation markers (i.e., CD80 and ICOSLG)
 based on mitochondrial size. We observed strong positive correlations

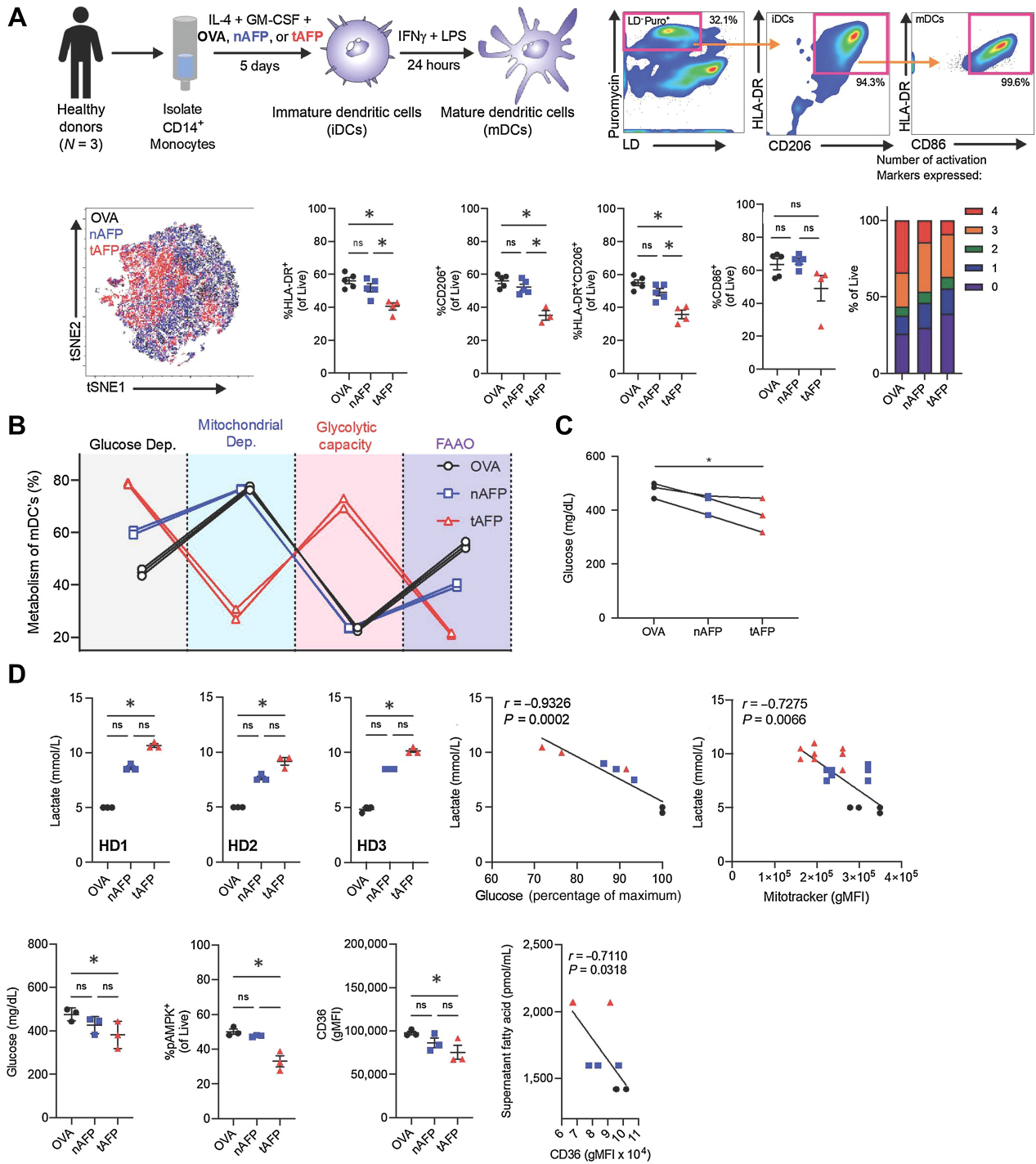
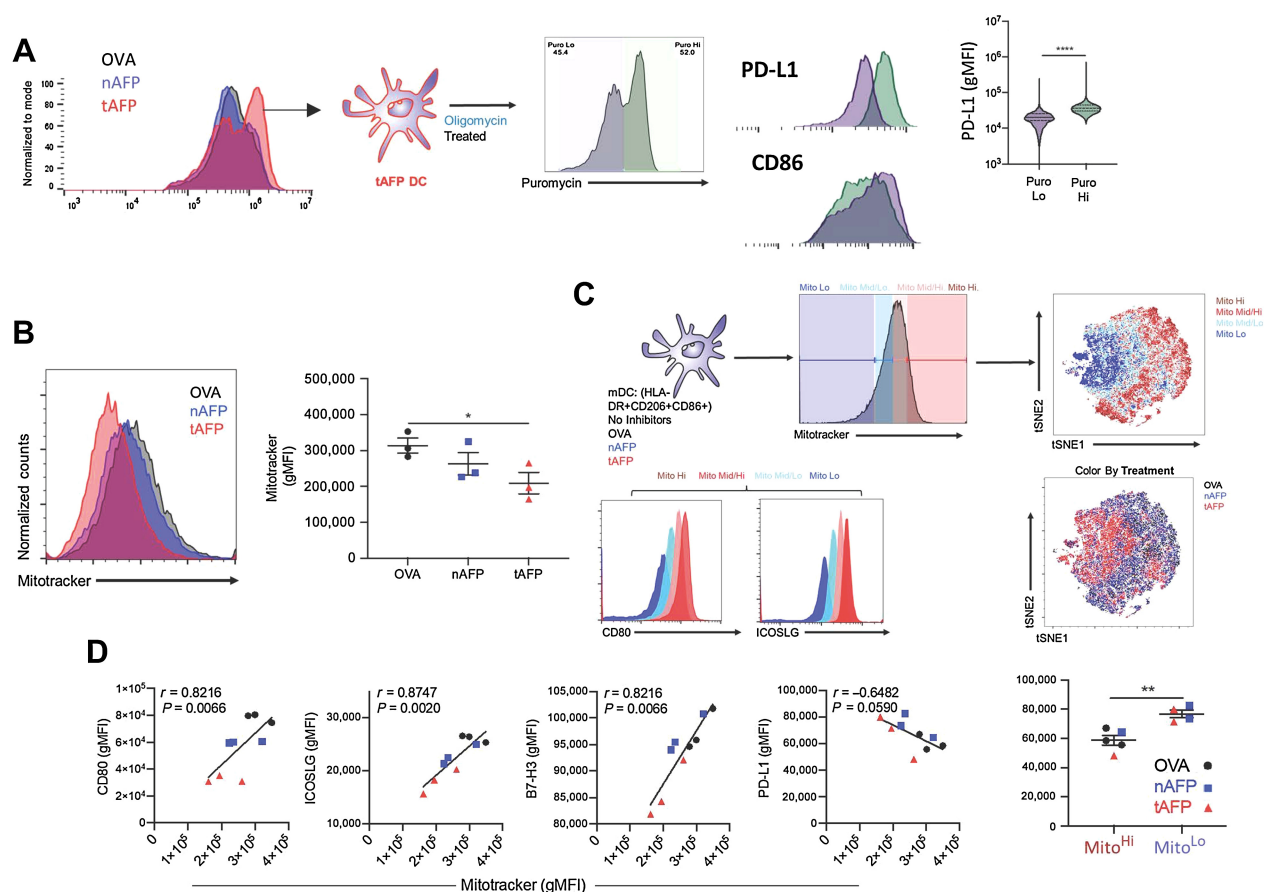


Figure 1.

tAFP exposure skews dendritic cell (DC) metabolism to glucose dependency. CD14⁺ monocytes were isolated from healthy donors and treated with IL4 + GM-CSF in the presence of OVA, nAFP or tAFP to produce immature DCs (iDC) and in some experiments treated with IFN γ and LPS to produce mature DCs (mDCs). **A**, A representative gating scheme is shown to identify live cells containing puromycin, as well as expressing markers consistent with iDCs (HLA-DR and CD206) and mDCs (CD86; **A**). DCs treated with OVA (black), nAFP (blue), and tAFP (red) were clustered on the basis of their immune parameters by tSNE, as well as the percentage of live cells expressing HLA-DR, CD206, and CD86. The proportion of cells expressing HLA-DR, CD206, CD86, and ICOSLG is shown from 3 to 5 technical replicates from a single donor (**A**). **B**, Shown are 3 technical replicates of one healthy donor of a SCENITH assay to quantify the glucose dependency (black), mitochondrial dependency (blue), glycolytic capacity (red), and fatty acid and glutaminolysis (FAAO; purple) with mDCs treated with OVA (black), nAFP (blue) or tAFP (red). Glucose and concentrations of cellular supernatants and intracellular glucose are shown with three technical replicates from a single donor, as well as the intracellular glucose uptake as determined by the influx of the fluorescent glucose analogue 2NDBG from a single replicate from a single donor. **C**, Shown are cellular supernatants of *in vitro* generated DCs from 3 healthy donors performed in technical replicates, as well as correlations with glucose in the supernatant and mitochondrial size. **D**, The glucose supernatant concentrations, %pAMPK, and CD36 gMFI are shown from healthy donors (N = 3) treated with OVA, nAFP or tAFP. The correlation between supernatant fatty acids and CD36 levels are shown.

**Figure 2.**

Mitochondria expression correlates with costimulatory molecule expression. Shown are puromycin histograms (a measurement of translation and a surrogate for ATP production) for OVA (black), nAFP (blue) or tAFP (red)-treated DCs. tAFP-treated DCs treated with oligomycin were separated into puromycin low (purple) and high (green). The expression levels of PD-L1 and CD86 are shown in the puromycin low and high DCs (**A**). Mitochondrial size, as measured by mitotracker was determined in OVA, nAFP, and tAFP-treated DCs (**B**). mDCs treated with OVA, nAFP, or tAFP were characterized by mitochondrial size with high (dark red), mid/high (pink), mid/low (teal), and low (dark blue), and clustered on the basis of immune parameters by tSNE colored by mitochondrial size or treatment condition. Shown are the expression levels of CD80 and ICOSLG based on mitochondrial size (**C**). Correlations between mitotracker and CD80, ICOSLG, B7-H3, and PD-L1 are shown. Differences in PD-L1 expression levels are shown between mito hi and mito lo cells color coded by treatment condition (**D**). All data are from one donor performed in 3 technical replicates.

404 between mitochondrial size and the expression of CD80 ($r = 0.8216$,
405 $P = 0.0066$), ICOSLG ($r = 0.8747$, $P = 0.0020$), and B7-H3/CD276 ($r =$
406 0.8216 , $P = 0.0066$; **Fig. 2C**). Although there was a trend toward
407 a negative correlation between mitochondrial size and PD-L1/CD274
408 ($r = -0.6482$, $P = 0.0590$), this reached statistical significance when
409 directly comparing PD-L1 levels between Mito^{Hi} versus Mito^{Lo} cells
410 (**Fig. 2D**). These findings indicate that decreased mitochondrial mass
411 skews the cells toward glycolysis and is also associated with weaker
412 expression of activating ligands (CD80, ICOSLG, B7-H3) and
413 increased expression of inhibitory ligands (PD-L1).

414 Single-cell phenotypic profiling

415 To further dissect the metabolic molecular pathways affected by
416 AFP, we used the recently described single-cell metabolic regulome
417 profiling (scMEP; ref. 42) on OVA, nAFP, and tAFP-treated cells.
418 Consistent with a less differentiated phenotype and with our previous
419 studies^{21,22}, tAFP DC had reduced expression of DC markers, includ-
420 ing CD206, PD-L1, CD11b, CD11c, HLA-DR, CD86, and CD11c

(**Fig. 3A**). Multiple metabolic parameters related to the electron
422 transport chain (ETC)/TCA, including ATP5A, CS and SDHA, were
423 lower in tAFP-treated cells (**Fig. 3B**). However, levels of cytochrome C
424 (CytC) were elevated in both nAFP and tAFP-treated DCs (**Fig. 3B**).
425 Fatty acid oxidation (FAO) associated or fatty acid synthase (FAS)
426 proteins CD36, CDPT1A, HADHA, and ACLY were decreased in
427 tAFP-treated mDCs. Proteins involved in amino acid (AA) pathways
428 had modest changes, CD98 and G6PD were significantly decreased
429 and GLS tended to be lower, whereas ASCT2 was unchanged (**Fig. 3B**).
430 Proteins involved in glycolysis (GLUT1, GLUT3, LDHA, ENO1,
431 GAPDH, and MTC1) displayed modest differences that were not
432 statistically significant. A schematic summarizing the proteins that
433 were upregulated, unchanged or downregulated is shown (**Fig. 3C**). A
434 heatmap with hierarchical clustering on the basis of metabolic markers
435 (FAO, AA, and ETC/TCA) and treatment condition (**Fig. 3D**). The
436 tAFP-treated mDC cluster separately from the nAFP or OVA-treated
437 mDCs. This clustering was due in large part to FAO and ETC/TCA
438 proteins CPT1A, HADHA, ACLY, CS, and ATP5A.
439

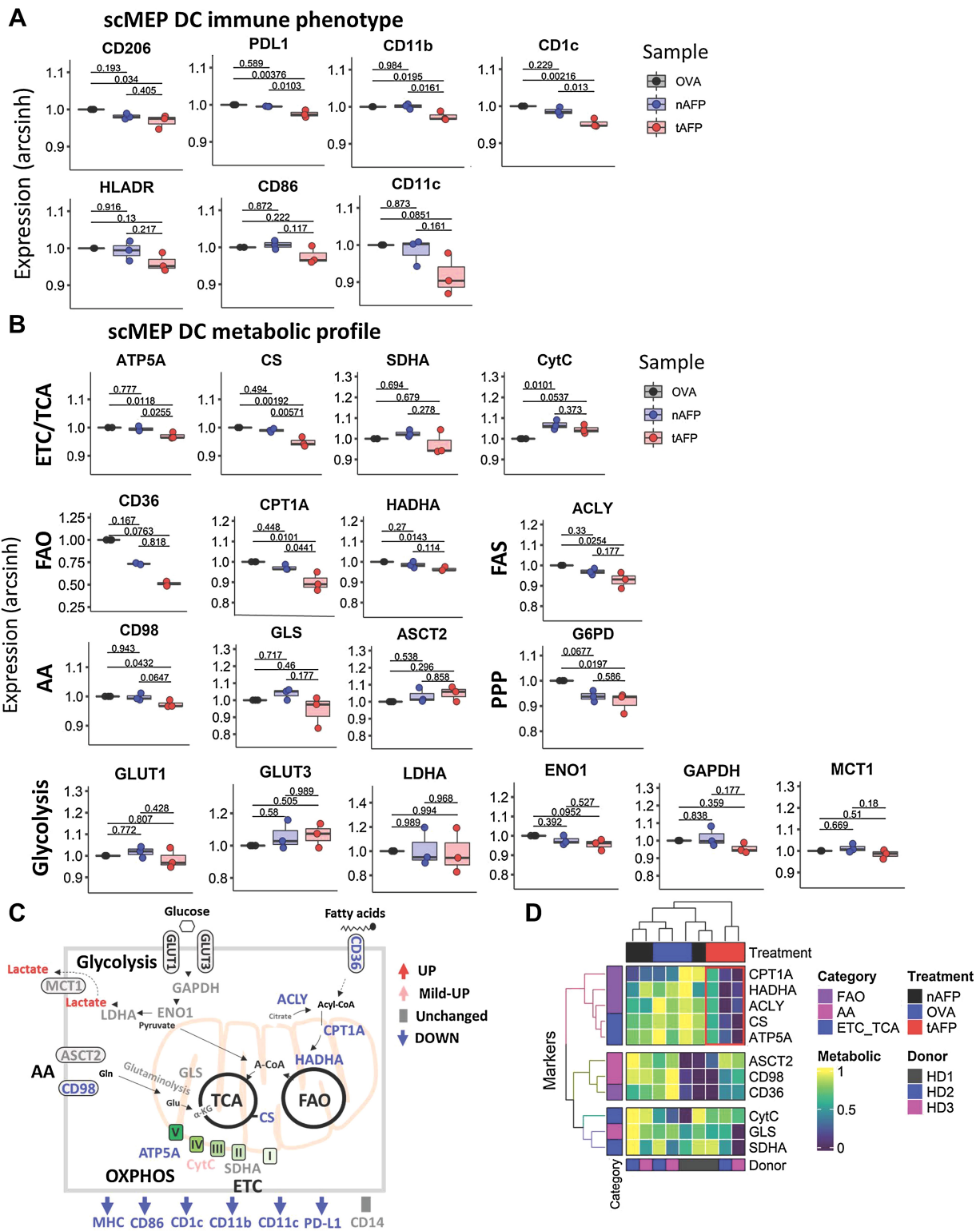


Figure 3.

Immune and metabolic profile by scMEP. mDC were generated *in vitro* in the presence of OVA, nAFP, tAFP and analyzed the immune-metabolic profile was determined by scMEP using CyTOF. Shown are the arc sinh-transformed values for immune response related molecules (A), and metabolic pathway proteins (B). A schematic is shown to summarize the tAFP-induced immune-metabolic changes (C). A heatmap of various metabolic markers was generated and hierarchical clustering was performed on the basis of marker expression and treatment condition. The red box indicates the unique clustering of the tAFP-treated cells (D). Data are representative of three separate healthy donors each performed in a single replicate.

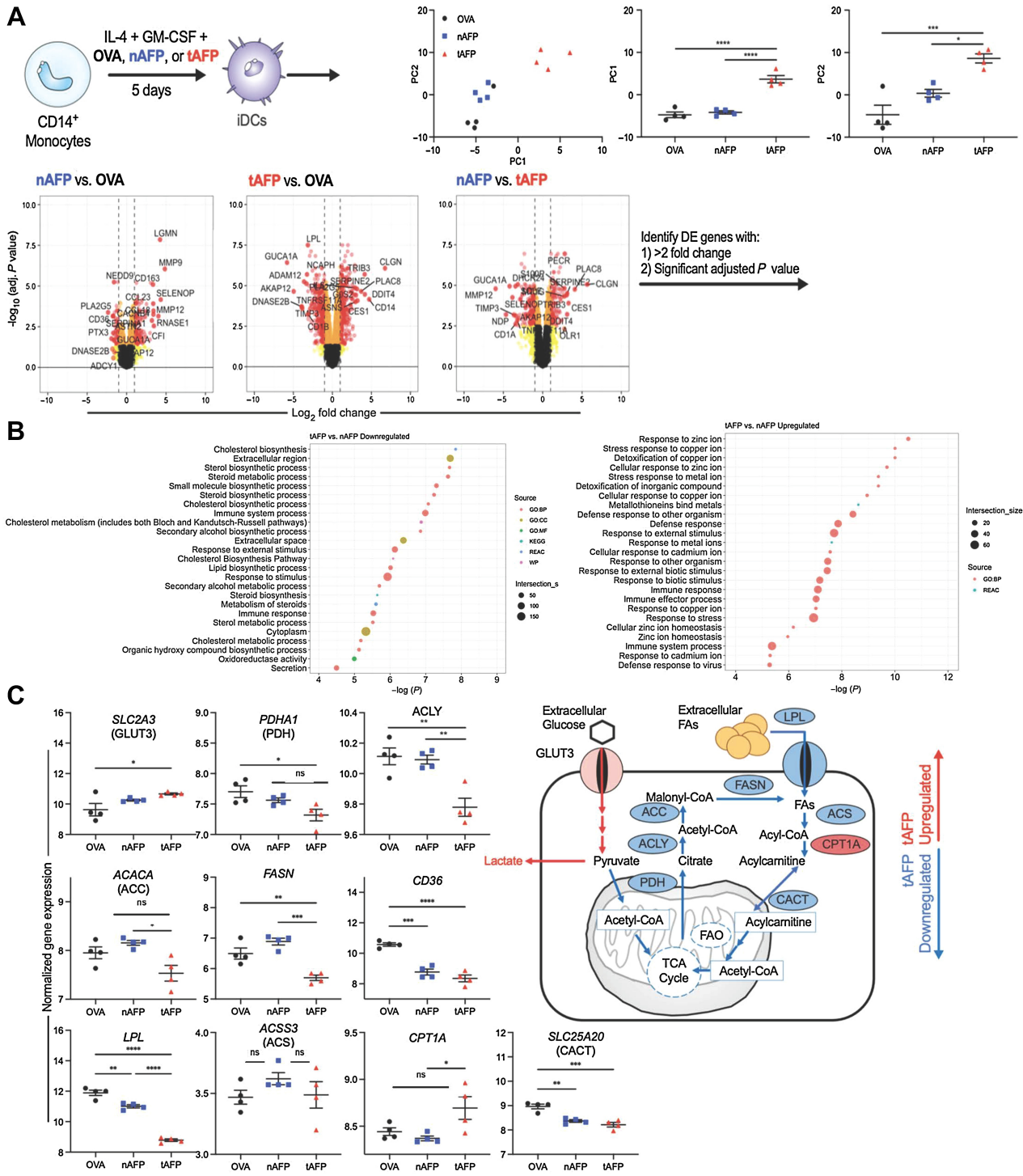


Figure 4.

DC gene expression profiles. Monocytes from healthy donors ($N = 4$) were differentiated into iDCs in the presence of OVA, nAFP, and tAFP and gene expression profiles were determined by microarray. Principle components were determined, and color coded by treatment condition. Volcano plots were generated to identify genes that were differentially enriched (>2 -fold change, significant adjusted P value) and that list of genes was used in a functional enrichment analysis by g:Profiler (A). Shown are predicted upregulated and downregulated pathways between tAFP and nAFP (B). Show are differences in genes involved in glycolysis and fatty acid metabolism pathways, and a schematic summary of tAFP upregulated (red) and downregulated (blue) genes (C). Data are from 4 healthy donors each performed once.

442 **tAFP induces transcriptional changes consistent with PUFA** 443 **exposure**

444 Given the AFP-induced protein level changes in multiple transcrip-
445 tion factors, we determined the tAFP-induced transcriptional changes
446 in DCs by microarray (Fig. 4). Principle component (PC) analysis
447 revealed tAFP clustered separately from OVA and nAFP, and PC1 and
448 PC2 were independently significant (Fig. 4A). We developed volcano
449 plots for the three possible comparisons to determine differentially
450 expressed genes (DEG). Consistent with the metabolic data, analysis
451 revealed that pathways associated with lipid metabolism were signif-
452 icantly downregulated in tAFP compared with nAFP. The upregulated
453 gene pathways demonstrated a stress response to metal ions, particu-
454 larly zinc (Fig. 4B).

455 To dissect these classifications, we analyzed individual genes that
456 could be important in promoting glycolysis and downregulated FA
457 uptake or oxidation. Consistent with tAFP decreasing free glucose in
458 the media and increasing lactate concentrations, we observed an
459 increase in *SLC2A3* (*GLUT3*) gene expression (Fig. 4C). In contrast,
460 we observed a consistent tAFP-induced downregulation with genes
461 involved in fatty acid metabolism, including genes encoding PDH,
462 *ACLY*, *ACC*, *FASN*, *LPL*, *CD36*, and *CACT* (Fig. 4C). Interestingly,
463 the *ACS* gene did not reach statistical significance, and tAFP
464 increased the gene expression of *CPT1A*. Overall, these data provide
465 strong orthogonal evidence in agreement with the SCENITH and
466 scMEP experiments that tAFP alters fatty acid metabolism at the
467 transcript level.

468 **tAFP ligands are enriched for zn and PUFAs**

469 To further define the mechanism by which tAFP alters metabolism
470 and function of DC (more so than nAFP), we examined the AFP-
471 bound LMM ligands (29) that we previously demonstrated altered
472 immunoregulatory properties of tAFP²². nAFP has been previously
473 shown to bind more polyunsaturated fatty acids (PUFA; ref. 49) and
474 zinc (Zn; refs. 39, 40) than albumin. Zn can induce tolerogenic DC (50),
475 and PUFAs are known inhibitors of DC differentiation (51) and have
476 previously been shown to limit lipid metabolism in hepatocytes, in
477 particular through the direct downregulation of the *FASN* gene. These
478 findings, taken together, suggest that the tAFP may bind more Zn and
479 PUFAs compared with nAFP, and therefore result in more potent
480 immuno-metabolic changes.

481 On the basis of the g-Profiler Zn gene signature (Fig. 4B), we
482 quantified the amount of intracellular Zn in OVA, nAFP, and tAFP-
483 treated iDCs. Monocytes were differentiated to iDCs in the presence of
484 OVA, nAFP, or tAFP. The tAFP-treated DC had a statistically
485 significant approximately 30% increase in Zn MFI compared with
486 nAFP ($P = 0.0293$) or OVA-treated ($P = 0.0228$) iDCs (Fig. 5A).
487 These findings are consistent the transcriptional data (Fig. 4), and
488 demonstrate that tAFP is more efficient at increasing intracellular Zn
489 concentrations in iDCs, when compared with OVA or nAFP.

490 OVA, nAFP, and tAFP LMM ligands were quantified by mass
491 spectrometry and gas chromatography. The total quantity of bound
492 fatty acids was similar among all proteins, with a mean concentration
493 of approximately 1,500 pmol/mL. In contrast, tAFP bound less
494 saturated fatty acids (SUFA; mean = 77%) compared with nAFP
495 (82%, $P = 0.0003$) or OVA (99%, $P < 0.0001$). Although the amount of
496 monounsaturated fatty acids (MUFA) was low among all proteins,
497 tAFP bound 2- and 4-fold more MUFAs compared with OVA ($P =$
498 0.0042) and nAFP ($P = 0.0318$), respectively (Fig. 5B). PUFAs were
499 greater on tAFP ($P < 0.0001$) and nAFP ($P = 0.0003$) when compared
500 with OVA. On the basis the terminal double-bond location, PUFAs
501 can be further divided into ω -3 and ω -6. Both tAFP ($P = 0.0067$) and

nAFP ($P = 0.0264$) had greater ω -3: ω -6 ratios than OVA. Next, we
503 examined each protein's ligand composition based upon the carbon
504 length and the number of double bonds of each FA. Although we did
505 not observe a bias based on FA length, nAFP and tAFP tended to bind
506 FAs with 4 or more double bonds. Next, we analyzed the proportion of
507 individual FAs from each protein (Fig. 5C). We hypothesized
508 that FAs present in high quantities in the media would be unlikely
509 to mediate tAFP's immunoregulatory properties, and FAs unique
510 to tAFP would be compelling candidates. To identify FAs statisti-
511 cally unique to tAFP, we generated volcano plots for all three
512 possible comparisons (Fig. 5D). Only a single fatty acid, 17:0, was
513 increased on OVA. As expected, both nAFP and tAFP bound
514 several PUFAs at a greater concentration relative to OVA. When
515 comparing nAFP and tAFP, PUFAs were enriched on nAFP (18:2,
516 18:3 N3) and tAFP (16:1, 20:3 N6, 22:5 N3, 20:5). To determine
517 which were shared or unique based on each comparison, a Euler
518 diagram of all the differentially bound fatty acids was generated
519 (Fig. 5E). Several of these differentially bound FAs were present in
520 the media (18:2, 18:3 N3, 16:1, 18:1) or attached equally to nAFP
521 and tAFP (20:4, 22:6, 22:5N6). However, the three fatty acids 20:5,
522 20:3 N6, 22:5N3 were statistically increased on tAFP and not
523 present in the other comparisons. 524

525 **PUFA restore tAFP's suppression of DCs**

526 We developed an *in vitro* assay to screen-specific FAs that are
527 necessary for tAFP-mediated suppression of DC formation (Fig. 6A;
528 Supplementary Fig. S2). Many of the FAs screened have known roles in
529 promoting (52, 53) or limiting DC differentiation (51). Therefore, to
530 determine their necessity for tAFP-mediated DC suppression, we
531 titrated several FAs unique to tAFP (20:3 N6, 20:5, and 22:5 N3), and
532 other PUFAs to determine the concentration they lost their inherent
533 ability to suppress DC differentiation in the absence of OVA, nAFP, or
534 tAFP (Fig. 6A). None of the FAs, at any concentration, tested induced
535 production of lactate to levels caused by tAFP, indicating that lactate
536 secretion and reduced costimulatory molecule expressions are sepa-
537 rable immune suppression effects. Treatment with high concentra-
538 tions (5–20 μ mol/L) of 16:0 (palmitic acid) tended to decrease the
539 production of lactate relative to control cells (black-dashed line),
540 suggesting a less glycolytic phenotype (Fig. 6B). All three PUFAs at
541 high concentrations inhibited CD206 expression on DCs (51), at levels
542 equivalent to or greater than tAFP treatment. In contrast, the SUFA
543 16:0 (palmitic acid) tended to promote DC differentiation (52). All
544 PUFAs lost immunoregulatory activity at the 0.2 μ mol/L concentra-
545 tion (Fig. 6B).

546 Although all of the PUFAs could inhibit CD206 expression of DC,
547 they did not robustly increase lactate production under these condi-
548 tions; in contrast, the saturated FA palmitic acid was unique in its
549 ability to increase CD206 expression and decrease lactate secretion
550 (Fig. 6A). None of the FAs combined with either OVA, nAFP or tAFP
551 induced lactate secretion comparable with native tAFP. When mea-
552 suring CD206 expression at the iDC stage, we observed immunoreg-
553 ulatory activity with FAs 20:3 N6 and 20:4 when combined with tAFP
554 —but not with OVA or nAFP (Fig. 6A). For mDC, we observed
555 inhibition (~15%) of CD206 expression with 20:3 N6, 20:4, and 22:4
556 when combined with tAFP (Fig. 6B). The more modest reduction at
557 the matured DC (matDC) timepoint suggests that treatment with
558 rIFN γ and LPS can partially, but not entirely reverse, the effects of
559 HMM tAFP + PUFAs. When multiple FA + HMM tAFP were
560 compared with controls, only 20:3N6 and 20:4 showed significantly
561 reduced CD206 expression (Fig. 6B). Importantly, in the metabolism
562 of ω -6 FAs, 20:3 N6 is converted to 20:4, which can then be further

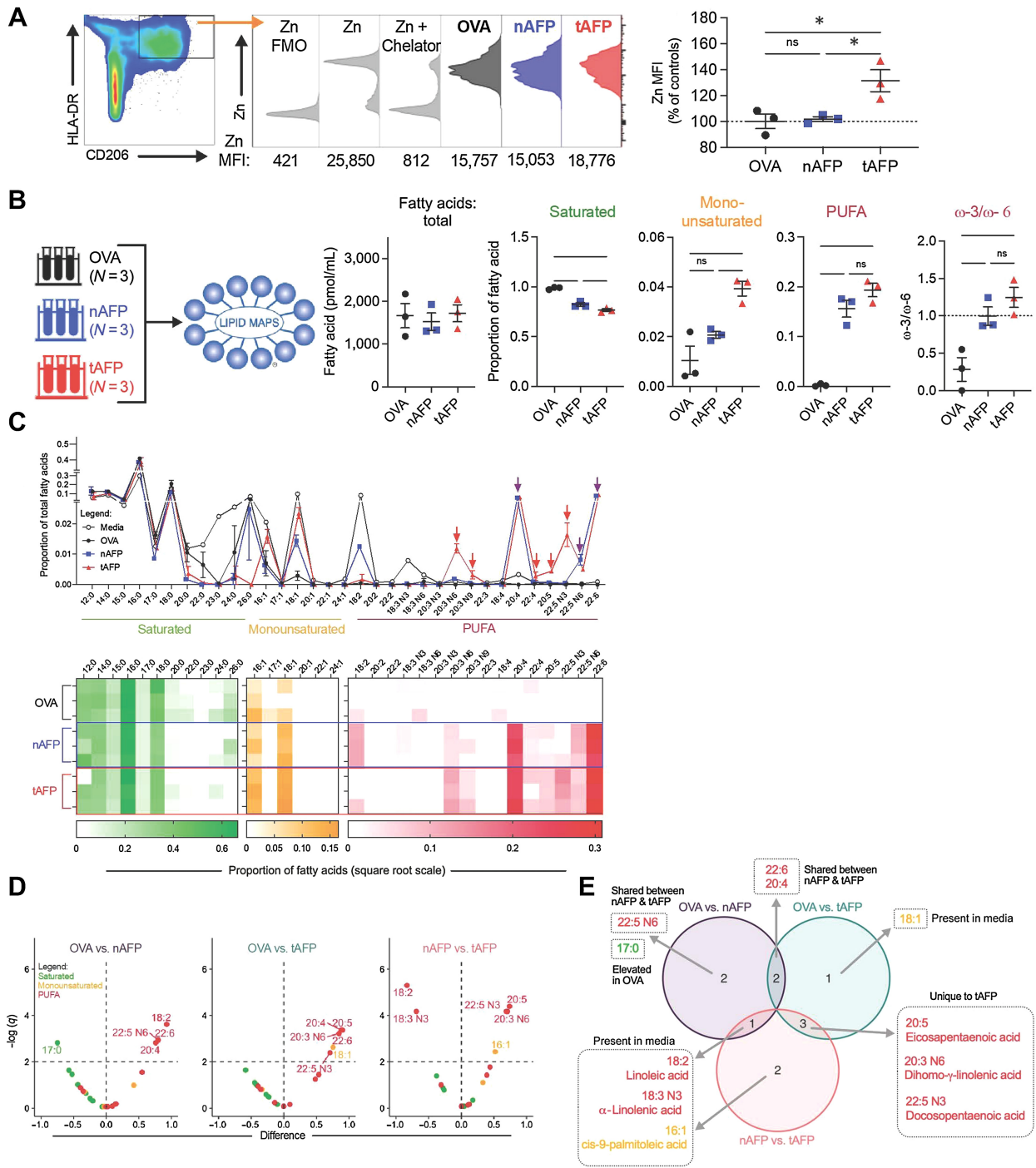


Figure 5. tAFP bound lipids are enriched for PUFAs. Levels of zinc were quantified in iDCs treated with OVA (black), nAFP (blue) or tAFP (red) in 3 technical replicates from a single donor and are shown as histograms as well as Zn MFIs (percentage of controls; **A**). Shown are the total mass of all bound fatty acids and the proportion that are saturated, monounsaturated, and polyunsaturated (PUFA) fatty acids (**B**). Displayed are the proportions of individual fatty acids present in CellGenix DC media, OVA, nAFP, or tAFP (**C**). Shown is a heatmap of the proportion of individual fatty acids bound to each protein (**C**). Volcano plots were generated on the basis of each protein compared with each other protein and color-coded on the basis of the class of fatty acid: Saturated (green), monounsaturated (yellow), and PUFA (red; **D**). The horizontal-dashed line indicates the significance threshold based on an FDR of 1%. An Euler diagram demonstrates the various combinations of differentially bound fatty acids (from **C**), indicating that are present in the media and are unique or shared amongst the proteins (**D**). Error bars are based on mean \pm standard deviation. Statistical differences in the mass or proportion of saturated, monounsaturated, or polyunsaturated fatty acids were determined on the basis of a one-way ANOVA with Tukey's multiple comparison test. Volcano plots were generated based upon unpaired *t* tests using a single pooled variance; multiple comparisons were accounted for using an FDR of 1% via a two-stage step-up.

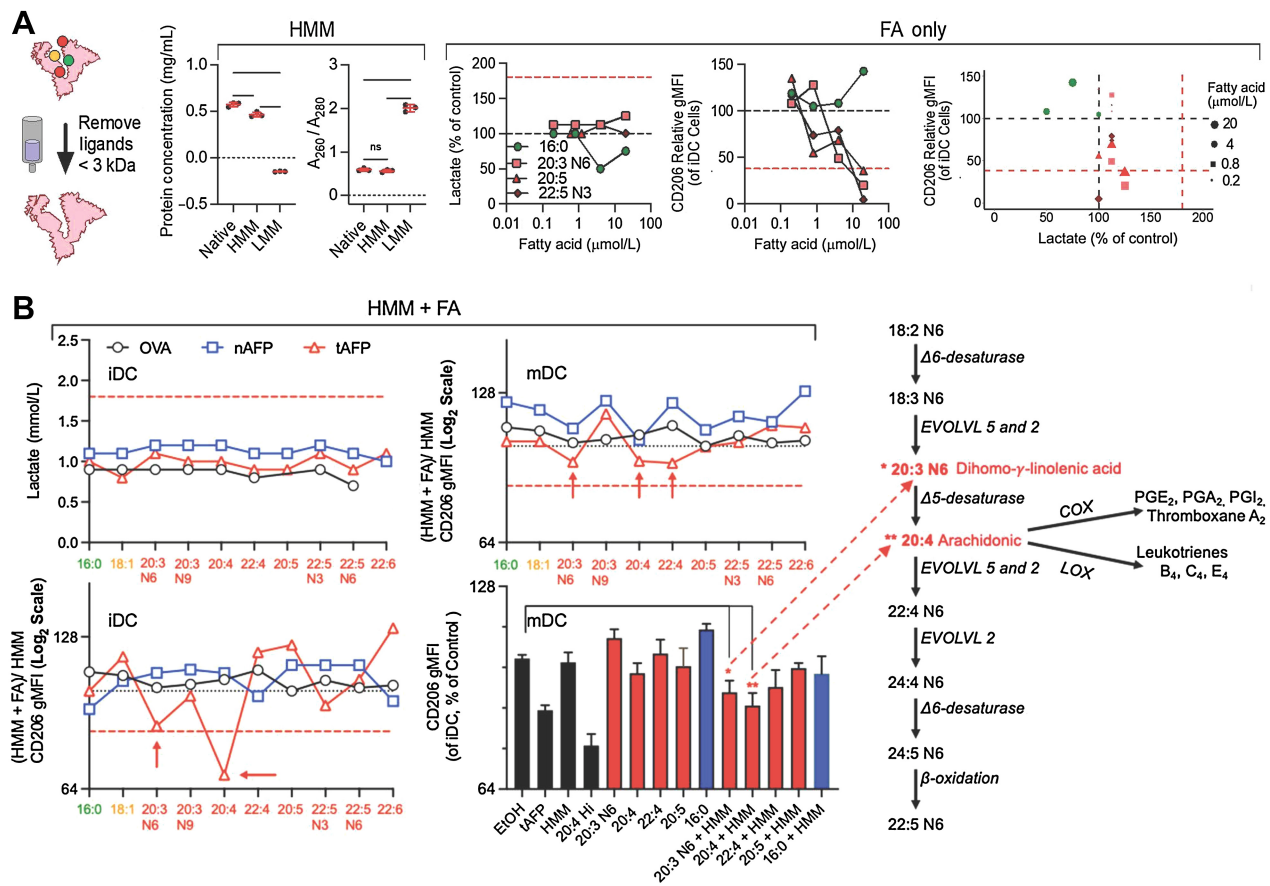


Figure 6.

Low molar mass-binding partner screening. Low molar mass ligands were removed from OVA, nAFP and tAFP (A). Fatty acids (FA) were titrated onto iDCs and supernatant lactate was measured. Control levels are indicated by a black-dashed line and native tAFP lactate induction indicated by a red-dashed line. Levels of CD206 were also measured with black and red-dashed lines indicated control and native tAFP-treated cells, respectively (A). Individual fatty acids were added back to high molar mass (HMM) purified OVA, nAFP, and tAFP proteins and supernatant lactate and CD206 levels were measured at the iDC and mDC stage. CD206 gMFI of the HMM + FA were normalized to the HMM only control. The red-dashed line indicated the level of suppression seen with native tAFP (B). The red asterisks indicate the fatty acids most significantly associated with a decrease in CD206. Also shown is a schematic of their role in fatty acid metabolism. Data were performed with 1-3 technical replicates from one healthy donor.

565 converted into a variety of molecules by COX and LOX enzymes
566 (Fig. 6B). Taken together, these data suggest that PUFAs are necessary
567 for tAFP inhibition of DC differentiation *in vitro*. Furthermore, these
568 effects may result from exposure to increased 20:3 N6 and/or 20:4,
569 COX/LOX enzymatic derivatives of 20:4.

HCC patient monocyte and DC metabolic profiling

570 To better understand how these *in vitro* results extend to *in vivo*
571 circulating patient myeloid cells, we measured the immunometabolic
572 profile of patient with HCC and HD PBMCs. SCENITH was used
573 to determine the percentage of glycolytic capacity and FAAO (Fig. 7A
574 and B) across cell types. Monocytes were classified as classical
575 (CD14⁺CD16⁻, cMo), intermediate (CD14⁺CD16⁺, iMo) or non-
576 classical (CD14⁻CD16⁺, ncMo). Among the monocyte subsets, met-
577 abolic differences between HCC and HD were most consistent among
578 the cMo (Fig. 7A and B). cMo from patients with HCC had decreased
579 glucose and mitochondrial dependence and increased glycolytic
580 capacity and FAAO compared with HD (Fig. 7C). Patient-derived
581 classical monocytes resembled *in vitro*-differentiated DCs treated with
582 AFP (Fig. 1B), showing decreased mitochondrial dependency and

585 elevated glycolytic capacity. In contrast with the *in vitro*-generated
586 DCs, patients with HCC had decreased glucose dependence and
587 increased FAAO (Fig. 7D). These *in vivo* findings are in partial
588 contrast with the prior *in vitro* data that suggested AFP-treated DCs
589 were more glucose-dependent and had decreased FAAO (Fig. 1B).
590 Regardless of the source of DCs, both *in vitro* treatment with tAFP or
591 *ex vivo* derived from patients with HCC were associated with DCs
592 retaining a more monocyte-like metabolic phenotype, consistent with
593 tAFP impairing the immuno-metabolic reprogramming required for
594 generating immunostimulatory DCs.

595 Given the correlation between metabolic state and suppression of
596 key stimulatory molecules (Fig. 2), we measured immune markers on
597 cMo and DCs. The immunoglobulin-like transcript 3 (ILT3) is an
598 important inhibitory receptor expressed on multiple myeloid cells,
599 including monocytes and DCs (54–56). Consistent with a more
600 immunoregulatory phenotype, HCC cMo (Fig. 7E) and DCs
601 (Fig. 7F) expressed more ILT3 compared with HDs. Consistent with
602 the *in vitro* data, CD206 was decreased in HCC patient DCs. Inter-
603 estingly, and in contrast with the *in vitro* data, HCC DCs expressed less
604 PD-L1 (Fig. 7H). Although this may suggest a less immunoregulatory

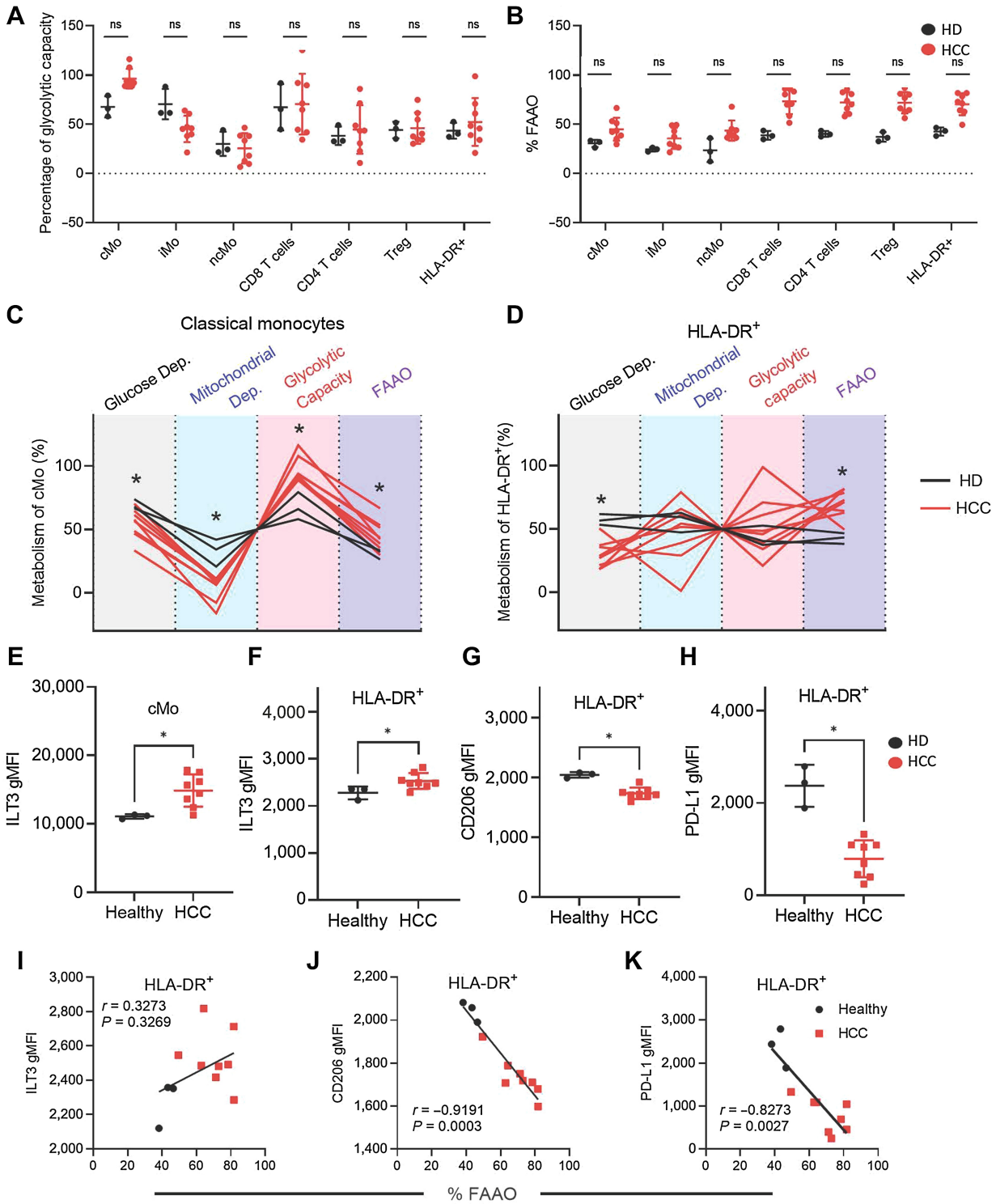


Figure 7.

Q9

HCC patient monocytes and DCs have a dysregulated immunometabolism. PBMCs were isolated from patients with hepatocellular carcinoma (HCC) for SCENITH analysis. Shown are the percentages of glycolytic capacity (**A**) and %FAAO (**B**) in multiple immune cell subsets (**A** and **B**). The total SCENITH metabolic profiles are shown for classic monocytes (**C**) and HLA-DR⁺ cells (**D**), with healthy donors (HD, in black) and HCC (in red), statistically significant differences are indicated with an asterisk. Levels of ILT3 are indicated on classical monocytes (cMo, **E**) and HLA-DR-positive cells (**F**). In addition, shown are CD206 and PD-L1 expression levels on HLA-DR⁺ cells (**G** and **H**). Correlations between ILT3 (**I**), CD206 (**J**), and PD-L1 (**K**) are shown with %FAAO in healthy donors (black circles) and patients with HCC (red squares). Data are representative from 3 healthy donors and 8 patients with HCC.

phenotype because immature DCs (iDC) tend to express less PD-L1 than matDCs, it could also result from a blockade in full DC differentiation (57). To understand the connection between these immune markers and their metabolic profiles, we performed correlations between these immune markers on DCs and the %FAAO. Although patients with HCC DCs tended to have greater %FAAO and ILT3 expression, these variables were not significantly correlated ($P = 0.3269$, $r = 0.3273$, Fig. 7I).

The serum concentration of AFP in patient blood (Table 1) did not show a direct correlation with circulating myeloid cell phenotypes or metabolic profiles (not shown). This may indicate that the type or amount of tumor-associated ligands binding tAFP *in vivo* vary between patients and tumors. This was not entirely unexpected, as our previous clinical trial analyses of DC vaccination, and of NK, CD8⁺, and CD4⁺ T-cell activity in AFP⁺ and AFP⁻ patients with HCC showed significant skewing and dysfunction that was not directly correlated to *in vivo* serum AFP concentrations (23, 24, 25, 58, 59, 60). Similarly, the tumor microenvironment concentrations of AFP are likely different from circulating concentrations.

Discussion

Here, using scMEP, we have identified key metabolic pathways and both transcriptional and protein-level regulatory molecules used by tAFP to suppress DC function. nAFP modestly increases glucose uptake and glucose-dependent metabolism and similarly reduces FAO. tAFP has a much more potent impact on DC metabolism, promoting a complete dysregulation of all measured metabolic pathways. tAFP-exposed DCs take up more glucose and secrete high levels of lactate, which is a well-recognized immune suppressive mediator (61, 62, 63). We recently showed that monocytes cultured in vitamin D3 to become functionally tolerogenic also have increased reliance on glycolysis and secrete high levels of lactate (48). Lactate blockade reversed the immune-suppressive phenotype of the tolerogenic DC. Here, we show that tAFP has a similar effect on DC.

We have also identified specific FA-binding partners of AFP that mediate some of these effects. These findings are consistent with groups that have shown that PUFAs inhibit DCs, some of these have been previously described (DPA, AA, and EPA) whereas others are newly described here (Dihomo-gamma). We also found consistent data that palmitic acid can promote DC differentiation and are the first to observe that palmitic acid can promote OxPhos. In our examination of the transcriptional pathways associated with Zn, our findings are consistent with groups who have shown Zn can induce tolerogenic DC. We now show that tAFP delivers more Zn intracellularly than nAFP and induces a glycolytic phenotype in DCs. Although AFP has been known to bind Zn, here, we report that the Zn bound to tAFP is important for the observed glycolytic switch.

It is important to consider is that metabolism of *in vitro* cultured DC may not fully reflect cellular metabolism in circulating cells *in vivo*, given the high concentration of glucose commonly present in culture media. Our comparative SCENITH analysis of HD and HCC PBMC revealed DCs that more closely resembled the metabolic profile of monocytes than of DCs. Both *in vitro*-generated DCs treated with tAFP and *ex vivo* DCs from patients with HCC had decreased mitochondrial dependency and increased glycolytic capacity when compared with controls. However, though *in vitro* generated DCs had increased glucose dependency and decreased

FAAO compared with controls, we saw the opposite pattern in HCC-derived DCs. Despite the similarities and differences between the *in vitro* and *ex vivo* DCs, in both instances, DCs treated with tAFP or derived from patients with HCC more closely resembled their respective monocyte metabolic profiles. These findings are consistent with tAFP limiting the immune-metabolic reprogramming during monocyte differentiation yielding DCs retaining monocyte profiles. Of note, there are several drugs (including TPST1120; ref. 64) being studied in HCC to inhibit PPARα and FAO. Such an approach could negatively impact the myeloid compartment and immune reactivity while targeting metabolic dysfunction in tumor cells, which could be investigated.

These data provide mechanistic insights on how AFP antagonizes the innate immune response to limit antitumor immunity *in vivo*. Understanding the impact of tAFP on the tumor immune microenvironment may inform the development of future immune checkpoint inhibition combination strategies in HCC overall and in the subset of patients with high tumor AFP expression. Furthermore, these data suggest novel strategies to generate more potent DC vaccines for patients with HCC, including supplementing culture media with SUFAs and inclusion of Zn chelators.

Authors' Disclosures

A.J. Combes reports grants from ImmunoX during the conduct of the study; and grants from Genentech, Eli Lilly, and Corbus outside the submitted work. R.K. Kelley reports grants from Agios, Astra Zeneca, Bayer, BMS, Eli Lilly, EMD Serono, Exelixis, as well as other support from Ipsen, and grants from Genentech/Roche, Merck, Novartis, Partner Therapeutics, QED, Relay Therapeutics, Surface Oncology, and personal fees from Kinnate and from Compass Therapeutics outside the submitted work. L.H. Butterfield reports grants from Parker Institute for Cancer Immunotherapy during the conduct of the study. No disclosures were reported by the other authors.

Authors' Contributions

P.V. Munson: Conceptualization, data curation, investigation, writing—original draft. J. Adamik: Conceptualization, data curation, formal analysis, investigation, writing—original draft, writing—review and editing. F.J. Hartmann: Investigation. P.M.B. Favaro: Investigation. D. Ho: Investigation. S.C. Bendall: Resources, supervision, writing—review and editing. A.J. Combes: Resources, investigation, writing—review and editing. M.F. Krummel: Resources, supervision, investigation. K. Zhang: Resources, writing—review and editing. R.K. Kelley: Resources, supervision, writing—original draft, writing—review and editing. L.H. Butterfield: Conceptualization, resources, supervision, funding acquisition, writing—original draft, project administration, writing—review and editing.

Acknowledgments

We wish to acknowledge the Hepatobiliary Tissue Bank Registry (HBTBR), which receives funding from the Bili Project Foundation, Inc. and the Cholangiocarcinoma Foundation; Dr. O. Quehenberger and Milda Simonaitis of the UCSF Lipidomics Core for the quantification of fatty acids; and Vinh Nguyen and Ashley Carlos of the UCSF Flow Cytometry Core for their consultation on flow cytometry assays (Ashley Carlos). This work was generously supported by the Parker Institute for Cancer Immunotherapy (PICI).

The publication costs of this article were defrayed in part by the payment of publication fees. Therefore, and solely to indicate this fact, this article is hereby marked "advertisement" in accordance with 18 USC section 1734.

Note

Supplementary data for this article are available at Cancer Research Online (<http://cancerres.aacrjournals.org/>).

Received November 12, 2022; revised January 4, 2023; accepted February 21, 2023; published first February 24, 2023.

72:Q12

728
729
730
731
732
733
734
735
736
737
738
739
740
741
742
743
744
745
746
747
748
749
750
751
752
753
754
755
756
757
758
759
760
761
762
763
764
765
766
767
768
769
770
771
772
773
774
775
776
777
778
779
780
781
782
783
784
785
786
787
788
789
790
791
792
793
794
795
796
797

References

- Sung H, Ferlay J, Siegel RL, Laversanne M, Soerjomataram I, Jemal A, et al. Global cancer statistics 2020: GLOBOCAN estimates of incidence and mortality worldwide for 36 cancers in 185 countries. *CA Cancer J Clin* 2021;71:209–49.
- Jemal A, Bray F, Center MM, Ferlay J, Ward E, Forman D. Global cancer statistics. *CA Cancer J Clin* 2011;61:69–90.
- Bertuccio P, Turati F, Carioli G, Rodriguez T, La Vecchia C, Malvezzi M, et al. Global trends and predictions in hepatocellular carcinoma mortality. *J Hepatol* 2017;67:302–9.
- R Team, LaBrecque DR, Abbas Z, Anania F, Ferenci P, Khan AG, et al. World Gastroenterology Organisation global guidelines: nonalcoholic fatty liver disease and nonalcoholic steatohepatitis. *J Clin Gastroenterol* 2014;48:467–73.
- Llovet JM, Kelley RK, Villanueva A, Singal AG, Pikarsky E, Roayaie S, et al. Hepatocellular carcinoma. *Nat Rev Dis Primer* 2021;7:6.
- Bruix J, Qin S, Merle P, Granito A, Huang Y-H, Bodoky G, et al. Regorafenib for patients with hepatocellular carcinoma who progressed on sorafenib treatment (RESORCE): a randomised, double-blind, placebo-controlled, phase 3 trial. *Lancet Lond Engl* 2017;389:56–66.
- Kudo M, Finn RS, Qin S, Han K-H, Ikeda K, Piscaglia F, et al. Lenvatinib versus sorafenib in first-line treatment of patients with unresectable hepatocellular carcinoma: a randomised phase 3 non-inferiority trial. *Lancet Lond Engl* 2018;391:1163–73.
- Finn RS, Qin S, Ikeda M, Galle PR, Ducreux M, Kim T-Y, et al. Atezolizumab plus bevacizumab in unresectable hepatocellular carcinoma. *N Engl J Med* 2020;382:1894–905.
- Finn RS, Cheng A-L. Atezolizumab and bevacizumab in hepatocellular carcinoma. *reply*. *N Engl J Med* 2020;383:695.
- Yau T, Kang Y-K, Kim T-Y, El-Khoueiry AB, Santoro A, Sangro B, et al. Efficacy and safety of nivolumab plus ipilimumab in patients with advanced hepatocellular carcinoma previously treated with sorafenib: the CheckMate 040 randomized clinical trial. *JAMA Oncol* 2020;6:e204564.
- Zhu AX, Kang Y-K, Yen C-J, Finn RS, Galle PR, Llovet JM, et al. Ramucirumab after sorafenib in patients with advanced hepatocellular carcinoma and increased α -fetoprotein concentrations (REACH-2): a randomised, double-blind, placebo-controlled, phase 3 trial. *Lancet Oncol* 2019;20:282–96.
- Llovet JM, Ricci S, Mazzaferro V, Hilgard P, Gane E, Blanc J-F, et al. Sorafenib in advanced hepatocellular carcinoma. *N Engl J Med* 2008;359:378–90.
- Finn RS, Qin S, Ikeda M, Galle PR, Ducreux M, Kim T-Y, et al. IMbrave150: updated overall survival (OS) data from a global, randomized, open-label phase III study of atezolizumab (atezo) + bevacizumab (bev) versus sorafenib (sor) in patients (pts) with unresectable hepatocellular carcinoma (HCC). *J Clin Oncol* 2021;39:267–.
- Finn RS, Ikeda M, Zhu AX, Sung MW, Baron AD, Kudo M, et al. Phase Ib study of lenvatinib plus pembrolizumab in patients with unresectable hepatocellular carcinoma. *J Clin Oncol Off J Am Soc Clin Oncol* 2020;38:2960–70.
- Kelley RK, Sangro B, Harris W, Ikeda M, Okusaka T, Kang Y-K, et al. Safety, efficacy, and pharmacodynamics of tremelimumab plus durvalumab for patients with unresectable hepatocellular carcinoma: randomized expansion of a phase I/II study. *J Clin Oncol Off J Am Soc Clin Oncol* 2021;39:2991–3001.
- Abou-Alfa GK, Lau G, Kudo M, Chan SL, Kelley RK, Furuse J, et al. Tremelimumab plus durvalumab in unresectable hepatocellular carcinoma. *NEJM Evid* 2022;1. Available from: <https://evidence.nejm.org/doi/10.1056/EVIDoa2100070>.
- Bai D-S, Zhang C, Chen P, Jin S-J, Jiang G-Q. The prognostic correlation of AFP level at diagnosis with pathological grade, progression, and survival of patients with hepatocellular carcinoma. *Sci Rep* 2017;7:12870.
- Hoshida Y, Moeini A, Alsinet C, Kojima K, Villanueva A. Gene signatures in the management of hepatocellular carcinoma. *Semin Oncol* 2012;39:473–85.
- Montal R, Andreu-Oller C, Bassaganyas L, Esteban-Fabro R, Moran S, Montironi C, et al. Molecular portrait of high alpha-fetoprotein in hepatocellular carcinoma: implications for biomarker-driven clinical trials. *Br J Cancer* 2019;121:340–3.
- Tatarinov IS. [Detection of embryo-specific alpha-globulin in the blood serum of a patient with primary liver cancer]. *Vopr Med Khim* 1964;10:90–1.
- Kelley RK, Meyer T, Rimassa L, Merle P, Park J-W, Yau T, et al. Serum alpha-fetoprotein levels and clinical outcomes in the phase III CELESTIAL study of cabozantinib versus placebo in patients with advanced hepatocellular carcinoma. *Clin Cancer Res Off J Am Assoc Cancer Res* 2020;26:4795–804.
- Farinati F, Marino D, De Giorgio M, Baldan A, Cantarini M, Cursaro C, et al. Diagnostic and prognostic role of alpha-fetoprotein in hepatocellular carcinoma: both or neither? *Am J Gastroenterol* 2006;101:524–32.
- Butterfield LH, Koh A, Meng W, Vollmer CM, Ribas A, Disette V, et al. Generation of human T-cell responses to an HLA-A2.1-restricted peptide epitope derived from alpha-fetoprotein. *Cancer Res* 1999;59:3134–42.
- Butterfield LH, Ribas A, Meng WS, Disette VB, Amarnani S, Vu HT, et al. T-cell responses to HLA-A*0201 immunodominant peptides derived from α -fetoprotein in patients with hepatocellular cancer. *Clin Cancer Res* 2003;9:5902–8.
- Butterfield LH, Ribas A, Disette VB, Lee Y, Yang JQ, De la Rocha P, et al. A phase I/II trial testing immunization of hepatocellular carcinoma patients with dendritic cells pulsed with four alpha-fetoprotein peptides. *Clin Cancer Res* 2006;12:2817–25.
- Vujanovic L, Stahl EC, Pardee AD, Geller DA, Tsung A, Watkins SC, et al. Tumor-derived α -fetoprotein directly drives human natural killer-cell activation and subsequent cell death. *Cancer Immunol Res* 2017;5:493–502.
- Lu CY, Changelian PS, Unanue ER. Alpha-fetoprotein inhibits macrophage expression of Ia antigens. *J Immunol* 1984;132:1722–7.
- Aussel C, Fehlmann M. α -Fetoprotein stimulates leukotriene synthesis in P388D1 macrophages. *Cell Immunol* 1986;101:415–24.
- Pardee AD, Shi J, Butterfield LH. Tumor-derived α -fetoprotein impairs the differentiation and T-cell stimulatory activity of human dendritic cells. *J Immunol* 2014;193:5723–32.
- Santos PM, Menk AV, Shi J, Tsung A, Delgoffe GM, Butterfield LH. Tumor-derived α -fetoprotein suppresses fatty acid metabolism and oxidative phosphorylation in dendritic cells. *Cancer Immunol Res* 2019;7:1001–12.
- Docta RY, Ferronha T, Sanderson JP, Weissensteiner T, Pope GR, Bennett AD, et al. Tuning T-cell receptor affinity to optimize clinical risk-benefit when targeting alpha-fetoprotein-positive liver cancer. *Hepatology* 2019;69:2061–75.
- Zhu W, Peng Y, Wang L, Hong Y, Jiang X, Li Q, et al. Identification of α -fetoprotein-specific T-cell receptors for hepatocellular carcinoma immunotherapy. *Hepatology* 2018;68:574–89.
- Vessella RL, Santrach MA, Bronson D, Smith CJP, Klicka MJ, Lange PH. Evaluation of AFP glycosylation heterogeneity in cancer patients with AFP-producing tumors. *Int J Cancer* 1984;34:309–14.
- Aoyagi Y, Suzuki Y, Isemura M, Nomoto M, Sekine C, Igarashi K, et al. The fucosylation index of alpha-fetoprotein and its usefulness in the early diagnosis of hepatocellular carcinoma. *Cancer* 1988;61:769–74.
- Lamerz R. AFP isoforms and their clinical significance (overview). *Anticancer Res* 1997;17:2927–30.
- Mizejewski GJ. Alpha-fetoprotein structure and function: relevance to isoforms, epitopes, and conformational variants. *Exp Biol Med Maywood NJ* 2001;226:377–408.
- Burditt LJ, Johnson MM, Johnson PJ, Williams R. Detection of hepatocellular carcinoma-specific alpha-fetoprotein by isoelectric focusing. *Cancer* 1994;74:25–9.
- Benassayag C, Vallette G, Delorme J, Savu L, Nunez EA. High affinity of nonesterified polyunsaturated fatty acids for rat alpha-fetoprotein (AFP). *OncoDev Biol Med* 1980;1:27–36.
- Wu JT, Monir-Vaghefi SM, Clayton F. Human alpha-fetoprotein and albumin: differences in zinc binding. *Clin Physiol Biochem* 1987;5:85–94.
- Permyakov SE, Oberg KA, Cherskaya AM, Shavlovsky MM, Permyakov EA, Uversky VN. Human alpha-fetoprotein as a Zn(2+)-binding protein. Tight cation binding is not accompanied by global changes in protein structure and stability. *Biochim Biophys Acta* 2002;1586:1–10.
- Argüello RJ, Combes AJ, Char R, Gigan J-P, Baaziz AI, Bousiquot E, et al. SCENITH: a flow cytometry-based method to functionally profile energy metabolism with single-cell resolution. *Cell Metab* 2020;32:1063–75.
- Hartmann FJ, Mrdjen D, McCaffrey E, Glass DR, Greenwald NF, Bharadwaj A, et al. Single-cell metabolic profiling of human cytotoxic T cells. *Nat Biotechnol* 2021;39:186–97.
- Hahne F, LeMeur N, Brinkman RR, Ellis B, Haaland P, Sarkar D, et al. flowCore: a Bioconductor package for high throughput flow cytometry. *BMC Bioinformatics*. 2009;10:106.
- Nowicka M, Krieg C, Crowell HL, Weber LM, Hartmann FJ, Guglietta S, et al. CyTOF workflow: differential discovery in high-throughput high-dimensional cytometry datasets. *F1000Research*. 2017;6:748.
- Raudvere U, Kolberg L, Kuzmin I, Arak T, Adler P, Peterson H, et al. gProfiler: a web server for functional enrichment analysis and conversions of gene lists (2019 update). *Nucleic Acids Res* 2019;47:W191–8.
- Quehenberger O, Armando AM, Brown AH, Milne SB, Myers DS, Merrill AH, et al. Lipidomics reveals a remarkable diversity of lipids in human plasma. *J Lipid Res* 2010;51:3299–305.

799
800
801
802
803
804
805
806
807
808
809
810
811
812
813
814
815
816
817
818
819
820
821
822
823
824
825
826
827
828
829
830
831
832
833
834
835
836
837
838
839
840
841
842
843
844
845
846
847
848
849
850
851
852
853
854
855
856
857
858
859
860
861
862
863
864
865
866
867
868

871	47. Alsabeeh N, Chausse B, Kakimoto PA, Kowaltowski AJ, Shirihai O. Cell culture models of fatty acid overload: problems and solutions. <i>Biochim Biophys Acta</i> 2018;1863:143–51.	900
872		901
873		902
874	48. Adamik J, Munson PV, Hartmann FJ, Combes AJ, Pierre P, Krummel MF, et al. Distinct metabolic states guide maturation of inflammatory and tolerogenic dendritic cells. <i>Nat Commun</i> 2022;13:5184.	903
875		904
876		905
877	49. Parmelee DC, Evenson MA, Deutsch HF. The presence of fatty acids in human alpha-fetoprotein. <i>J Biol Chem</i> 1978;253:2114–9.	906
878		907
879	50. George MM, Subramanian Vignesh K, Landero Figueroa JA, Caruso JA, Deepe GS. Zinc induces dendritic cell tolerogenic phenotype and skews regulatory T-cell-Th17 balance. <i>J Immunol Baltim Md 1950</i> 2016;197:1864–76.	908
880		909
881		910
882	51. Zeyda M, Säemann MD, Stuhlmeier KM, Mascher DG, Nowotny PN, Zlabinger GJ, et al. Polyunsaturated fatty acids block dendritic cell activation and function independently of NF-κB activation. <i>J Biol Chem</i> 2005;280:14293–301.	911
883		912
884		913
885		914
886	52. Weatherill AR, Lee JY, Zhao L, Lemay DG, Youn HS, Hwang DH. Saturated and polyunsaturated fatty acids reciprocally modulate dendritic cell functions mediated through TLR4. <i>J Immunol</i> 2005;174:5390–7.	915
887		916
888		917
889	53. Lancaster GI, Langley KG, Berglund NA, Kammoun HL, Reibe S, Estevez E, et al. Evidence that TLR4 is not a receptor for saturated fatty acids but mediates lipid-induced inflammation by reprogramming macrophage metabolism. <i>Cell Metab</i> 2018;27:1096–110.e5.	918
890		919
891		920
892	54. Cella M, Döhning C, Samaridis J, Dessing M, Brockhaus M, Lanzavecchia A, et al. A novel inhibitory receptor (ILT3) expressed on monocytes, macrophages, and dendritic cells involved in antigen processing. <i>J Exp Med</i> 1997;185:1743–51.	921
893		922
894		923
895		924
896	55. Manavalan JS, Rossi PC, Vlad G, Piazza F, Yamilina A, Cortesini R, et al. High expression of ILT3 and ILT4 is a general feature of tolerogenic dendritic cells. <i>Transpl Immunol</i> 2003;11:245–58.	925
897		926
898		927
	56. Chang CC, Ciubotariu R, Manavalan JS, Yuan J, Colovai AI, Piazza F, et al. Tolerization of dendritic cells by T(S) cells: the crucial role of inhibitory receptors ILT3 and ILT4. <i>Nat Immunol</i> 2002;3:237–43.	
	57. Pen JJ, Keersmaecker BD, Heirman C, Corthals J, Liechtenstein T, Escors D, et al. Interference with PD-L1/PD-1 co-stimulation during antigen presentation enhances the multifunctionality of antigen-specific T cells. <i>Gene Ther</i> 2014;21:262–71.	
	58. Liu Y, Daley S, Evdokimova VN, Zdobinski DD, Potter DM, Butterfield LH. Hierarchy of alpha fetoprotein (AFP)-specific T-cell responses in subjects with AFP-positive hepatocellular cancer. <i>J Immunol Baltim Md 1950</i> 2006;177:712–21.	
	59. Evdokimova VN, Butterfield LH. Alpha-fetoprotein and other tumour-associated antigens for immunotherapy of hepatocellular cancer. <i>Expert Opin Biol Ther</i> 2008;8:325–36.	
	60. Evdokimova VN, Liu Y, Potter DM, Butterfield LH. AFP-specific CD4 ⁺ helper T-cell responses in healthy donors and HCC patients. <i>J Immunother Hagerstown Md</i> 1997 2007;30:425–37.	
	61. Certo M, Tsai C-H, Pucino V, Ho P-C, Mauro C. Lactate modulation of immune responses in inflammatory versus tumour microenvironments. <i>Nat Rev Immunol</i> 2021;21:151–61.	
	62. de la Cruz-López KG, Castro-Muñoz LJ, R-H DO, García-Carrancá A, Manzo-Merino J. Lactate in the regulation of tumor microenvironment and therapeutic approaches. <i>Front Oncol</i> 2019;9:1143.	
	63. Hirschhaeuser F, Sattler UGA, Mueller-Klieser W. Lactate: a metabolic key player in cancer. <i>Cancer Res</i> 2011;71:6921–5.	
	64. Yarchoan M, Powderly JD, Bastos BR, Karasic TB, Crysler OV, Munster PN, et al. A phase 1 study of TPST-1120 as a single agent and in combination with nivolumab in subjects with advanced solid tumors. <i>J Clin Oncol</i> 2022;40:3005–.	

AUTHOR QUERIES

AUTHOR PLEASE ANSWER ALL QUERIES

- Q1: Page: 1: Author: Per journal style, genes, alleles, loci, and oncogenes are italicized; proteins are roman. Please check throughout to see that the words are styled correctly. AACR journals have developed explicit instructions about reporting results from experiments involving the use of animal models as well as the use of approved gene and protein nomenclature at their first mention in the manuscript. Please review the instructions at <http://aacrjournals.org/content/authors/editorial-policies#genomen> to ensure that your article is in compliance. If your article is not in compliance, please make the appropriate changes in your proof.
- Q2: Page: 1: Author: Please verify the drug names and their dosages used in the article.
- Q3: Page: 1: Author: Please verify the affiliations and their corresponding author links.
- Q4: Page: 1: Author: Please verify the corresponding author details.
- Q5: Page: 2: Author: Please verify the layout of Tables for correctness.
- Q6: Page: 3: Author: Units of measurement have been changed here and elsewhere in the text from "M" to "mol/L," and related units, such as "mmol/L" and " μ mol/L," in figures, legends, and tables in accordance with journal style, derived from the Council of Science Editors Manual for Authors, Editors, and Publishers and the Système international d'unités. Please note if these changes are not acceptable or appropriate in this instance.
- Q7: Page: 5: Author: Please specify the significance of "*" appearing in the artwork of Fig. 1.
- Q8: Page: 5: Author: Please confirm quality/labeling of all images included within this article. Thank you.
- Q9: Page: 12: Author: Part 7E is not described in its respective figure caption. Please check.
- Q10: Page: 13: Author: The Authors' Disclosures statement that appears in the proof incorporates the information from forms completed and signed off on by each individual author. No factual changes can be made to disclosure information at the proof stage. However, typographical errors or misspelling of author names should be noted on the proof and will be corrected before publication. Please note if any such errors need to be corrected. Is the disclosure statement correct?
- Q11: Page: 13: Author: The contribution(s) of each author are listed in the proof under the heading "Authors' Contributions." These contributions are derived from forms completed and signed off on by each individual author. If you make changes to these contributions, you must inform the affected author(s).
- Q12: Page: 14: Author: Note that the references have been renumbered in both the text and the list to maintain the sequential order of reference citations in the text. Please verify.

AU: Below is a summary of the name segmentation for the authors according to our records. The First Name and the Surname data will be provided to PubMed when the article is indexed for searching. Please check each name carefully and verify that the First Name and Surname are correct. If a name is not segmented correctly, please write the correct First Name and Surname on this page and return it with your proofs. If no changes are made to this list, we will assume that the names are segmented correctly, and the names will be indexed as is by PubMed and other indexing services.

First Name	Surname
Paul V.	Munson
Juraj	Adamik
Felix J.	Hartmann
Patricia M.B.	Favaro
Daniel	Ho
Sean C.	Bendall
Alexis J.	Combes
Matthew F.	Krummel
Karen	Zhang
Robin K.	Kelley
Lisa H.	Butterfield